

An object oriented framework: From flexible multibody dynamics to fluid-structure interaction.

Christian Hesch and Peter Betsch

Chair of Computational Mechanics
University of Siegen
Paul-Bonatz-Str. 9-11, 57068 Siegen, Germany
[christian.hesch, peter.betsch]@uni-siegen.de

ABSTRACT

The development of complex simulation programs within a team of researchers requires not only knowledge of the underlying mechanics and the associated algorithms, but also a detailed planning of the interfaces within the program. In particular, an object oriented framework, used for the implementation in Matlab as well as in C++ and the combination thereof provide an effective tool for the requirements of a research team. In addition, it enables researchers to focus on their primary interests. Various examples including rigid bodies, deformable bodies and fluids demonstrate the capability of the implementation.

1 INTRODUCTION

We work with an object oriented framework within Matlab using C++ MEX files for the core functionalities to speed up the calculations. This allows us to set up an easy to handle system for engineers from different fields of research. This incorporation of various elements for rigid bodies (see Betsch & Uhlar [6]), geometrically exact beams (see Betsch & Steinmann [5]), geometric exact shells (see Betsch & Sanger [4]), deformable bodies (see Hesch & Betsch [10, 11]), thermoelastic systems (see Hesch & Betsch [12]), thermoviscoelastic systems (see Kruger et al. [16]), fluid-structure interaction problems (see Hesch et al. [15]) and phase field models (see Anders et al. [1]). We will focus on rigid and deformable bodies as well as on fluid-structure interaction problems in the present contribution.

2 Flexible multibody dynamics

In this and the subsequent sections we present in detail the mechanics of the chosen examples used within a unified mechanical framework and implemented in a common object oriented structure. First, we outline a uniform framework for flexible multibody dynamics that will be applied in the present work (see Betsch et al. [3]). In multibody dynamics it is common to use rotation parameters such as joint-angles, Euler angles, Euler parameters or unit quaternions for the description of the orientation of body-fixed frames. Here, we focus on a rotationless formulation (cf. Betsch [2, 6]) for all constraint systems.

2.1 Rigid body dynamics

Rather than using rotation variables for the parametrization of the nonlinear configuration manifold pertaining to a specific multibody system we make use of redundant coordinates subject to geometric constraints. Accordingly, we consider constrained finite dimensional mechanical systems, where $\mathbf{q} \in \mathbb{R}^n$ denotes the vector of redundant coordinates and $\boldsymbol{\lambda} \in \mathbb{R}^m$ the vector of Lagrange multipliers for the enforcement of the vector of constraints $\boldsymbol{\Phi} \in \mathbb{R}^m$. The uniform description of flexible multibody dynamics is characterized by the Lagrangian

$$L(\mathbf{q}, \dot{\mathbf{q}}) = \frac{1}{2} \dot{\mathbf{q}} \cdot \mathbf{M} \dot{\mathbf{q}} - V(\mathbf{q}) \quad (1)$$

where $\dot{\mathbf{q}}$ denotes the vector of redundant velocities, \mathbf{M} the symmetric and, more importantly, constant mass matrix. Typically, the potential function is split as follows $V(\mathbf{q}) = V^{int} + V^{ext}$, where V^{ext} is related to

external loads, and V^{int} accounts for hyperelastic material behavior, vanishing in the case of rigid bodies. Following the path of stationary action yields the set of differential-algebraic equations (DAEs)

$$\begin{aligned} M\ddot{\mathbf{q}} &= -\nabla V(\mathbf{q}) - \mathbf{G}^T(\mathbf{q})\boldsymbol{\lambda} \\ \Phi(\mathbf{q}) &= \mathbf{0} \end{aligned} \quad (2)$$

The holonomic constraints are assumed to be independent, so that the constraint Jacobian $\mathbf{G}(\mathbf{q}) = \nabla\Phi(\mathbf{q})$ has full row rank. Due to the presence of the holonomic constraints, the configuration space of the constrained mechanical system under consideration is given by

$$Q = \{\mathbf{q} \in \mathbb{R}^n \mid \Phi(\mathbf{q}) = \mathbf{0}\} \quad (3)$$

Kinematics To describe the kinematics (cf. Betsch & Uhlar [7]) of the free rigid body, we assume that $\mathbf{X} = X^i \mathbf{e}_i$ is a material point which belongs to the reference configuration $\mathcal{B}_0 \subset \mathbb{R}^3$ of the rigid body. The spatial position of \mathbf{X} at time $t \in \mathbb{I} := [0, T]$ is given by

$$\mathbf{x}(\mathbf{X}, t) = \boldsymbol{\varphi}(t) + X^i \mathbf{d}_i(t) \quad (4)$$

where $\boldsymbol{\varphi}(t) \in \mathbb{R}^3$ denotes the position of the center of mass and $\mathbf{d}_i(t) \in \mathbb{R}^3$ a body fixed director frame. It is obvious that the configuration of the rigid body is specified by the vector of coordinates

$$\mathbf{q} = [\boldsymbol{\varphi}^T, \mathbf{d}_1^T, \mathbf{d}_2^T, \mathbf{d}_3^T] \quad (5)$$

To enforce the rigidity of the body, we have to incorporate 6 holonomic constraints given by

$$\Phi_{int}(\mathbf{q}) = \begin{bmatrix} \frac{1}{2}(\mathbf{d}_1 \cdot \mathbf{d}_1 - 1) \\ \frac{1}{2}(\mathbf{d}_2 \cdot \mathbf{d}_2 - 1) \\ \frac{1}{2}(\mathbf{d}_3 \cdot \mathbf{d}_3 - 1) \\ \mathbf{d}_1 \cdot \mathbf{d}_2 \\ \mathbf{d}_1 \cdot \mathbf{d}_3 \\ \mathbf{d}_2 \cdot \mathbf{d}_3 \end{bmatrix} \quad (6)$$

One of the main distinguishing features of the rotationless rigid body formulation is the specific structure of the mass matrix

$$M = \begin{bmatrix} \mathcal{M}I & \mathbf{0} & \mathbf{0} & \mathbf{0} \\ \mathbf{0} & \mathcal{E}_1 I & \mathbf{0} & \mathbf{0} \\ \mathbf{0} & \mathbf{0} & \mathcal{E}_2 I & \mathbf{0} \\ \mathbf{0} & \mathbf{0} & \mathbf{0} & \mathcal{E}_3 I \end{bmatrix} \quad (7)$$

where I and $\mathbf{0}$ are the 3×3 identity and zero matrices, \mathcal{M} denotes the total mass of the rigid body and \mathcal{E}_i the principal values of the convected Euler tensor. The connection with the principal values of the convected inertia tensor is given by

$$\mathcal{E}_i = \frac{1}{2}(\mathcal{J}_j + \mathcal{J}_k - \mathcal{J}_i) \quad (8)$$

for even permutations of the indices i, j, k .

Equations of motion Following the above outlined structure of the DAEs in (2) we obtain the following set equations

$$\begin{aligned} \dot{\mathbf{q}} &= \mathbf{v} \\ M\dot{\mathbf{v}} &= -\nabla V^{ext}(\mathbf{q}) - \mathbf{G}^T(\mathbf{q})\boldsymbol{\lambda} \\ \Phi(\mathbf{q}) &= \mathbf{0} \end{aligned} \quad (9)$$

To solve the non-linear system using a Newton-Raphson iteration we apply an implicit time-stepping scheme. Accordingly, the full discrete equations read

$$\begin{aligned} \mathbf{q}_{n+1} - \mathbf{q}_n &= \frac{\Delta t}{2}(\mathbf{v}_{n+1} + \mathbf{v}_n) \\ M(\mathbf{v}_{n+1} - \mathbf{v}_n) &= -\Delta t \nabla V^{ext}(\mathbf{q}_{n+1/2}) - \mathbf{G}^T(\mathbf{q}_{n+1/2})\boldsymbol{\lambda}_{n+1} \\ \Phi(\mathbf{q}_{n+1}) &= \mathbf{0} \end{aligned} \quad (10)$$

This accomplish the rotationless formulation of rigid bodies. Within the object oriented framework each rigid body is represented by a single object which knows about its position and orientation as well as the corresponding contributions to the residual vector. Within the follow up section we extend the system to include deformable bodies, i.e. we insert an internal potential representing the local strain energy of the body.

2.2 Deformable continua

For deformable bodies within a Lagrangian framework we assume a similar mapping as before using $\varphi^{(i)}(\mathbf{X}^{(i)}, t)$ for each body $i \in [1 \dots k]$, characterizing the current position at time t . The corresponding mapping of the surface $\Gamma^{(i)}$ is denoted by $\gamma^{(i)} = \varphi(\Gamma^{(i)}, t)$. Note that we require that the boundaries satisfy

$$\Gamma_u^{(i)} \cup \Gamma_\sigma^{(i)} = \Gamma^{(i)} \quad \text{and} \quad \Gamma_u^{(i)} \cap \Gamma_\sigma^{(i)} = \emptyset \quad (11)$$

where $\Gamma_u^{(i)}$ and $\Gamma_\sigma^{(i)}$ denote the Dirichlet and Neumann boundaries, respectively. In the sequel we make use of the notation

$$\int_{\mathcal{B}^{(i)}} (\bullet) \cdot (\bullet) d\mathcal{B}^{(i)} =: \langle \bullet, \bullet \rangle^{(i)} \quad \text{and} \quad \int_{\Gamma^{(i)}} (\bullet) \cdot (\bullet) d\Gamma^{(i)} =: \langle \bullet, \bullet \rangle_{\Gamma}^{(i)} \quad (12)$$

The contribution of body (i) to the virtual work for a large deformation contact problem can be expressed as follows

$$G^{(i)}(\varphi, \delta\varphi) = \langle \rho_R \ddot{\varphi}, \delta\varphi \rangle^{(i)} + \langle \mathbf{P}, \nabla_{\mathbf{X}} (\delta\varphi) \rangle^{(i)} - \langle \rho_R \bar{\mathbf{B}}, \delta\varphi \rangle^{(i)} - \langle \bar{\mathbf{T}}, \delta\varphi \rangle_{\Gamma_\sigma}^{(i)} - \langle \mathbf{t}, \delta\varphi \rangle_{\Gamma_c}^{(i)} \quad (13)$$

where \mathbf{P} denotes the first Piola-Kirchhoff tensor and \mathbf{T} the external stresses at the Neumann boundary. To achieve a feasible numerical solution for the nonlinear problem under consideration, we apply a spatial discretization process to each body $\mathcal{B}^{(i)}$ by introducing a set of finite elements $e \in \mathbb{E}^h$ via

$$\mathcal{B}^{(i),h} = \bigcup_{\forall e \in \mathbb{E}^h} \mathcal{B}_e^{(i),h} \quad (14)$$

Using a standard displacement-based finite element approach, we introduce finite dimensional approximations of φ and $\delta\varphi$ given by

$$\varphi^{(i),h} = \sum_{A \in \mathcal{B}} N^A \mathbf{q}_A^{(i)}, \quad \text{and} \quad \delta\varphi^{(i),h} = \sum_{B \in \mathcal{B}} N^B \delta \mathbf{q}_B^{(i)} \quad (15)$$

where $\mathbf{q}_A^{(i)} = \varphi^{(i)}(\mathbf{X}_A^{(i)}, t)$, $A, B \in \mathcal{B} = \{1, \dots, n_{\text{node}}\}$ are the nodal values of the configuration mapping at time t . Furthermore, $N^A(\mathbf{X}^{(i)}) : \mathcal{B}^{(i),h} \rightarrow \mathbb{R}$ are the global shape functions associated with nodes A . The coefficients of the discrete mass matrix

$$\mathbf{M}^{AB} = \int_{\mathcal{B}} \rho_R N^A N^B dV \mathbf{I} \quad (16)$$

are now introduced together with the variations $\delta \mathbf{q}$ of the discrete configuration. For the virtual work of the internal forces, the discretized deformation gradient and deformation tensor have to be incorporated using

$$\mathbf{F}^{(i),h} = \frac{\delta \varphi^{(i),h}}{\delta \mathbf{X}^{(i)}} = \sum_{A \in \omega^{(i)}} \mathbf{q}_A^{(i)} \otimes \nabla N^A(\mathbf{X}^{(i)}) \quad (17)$$

and

$$\mathbf{C}^{(i),h} = \sum_{A, B \in \omega^{(i)}} \mathbf{q}_A^{(i)} \cdot \mathbf{q}_B^{(i)} \nabla N^A(\mathbf{X}^{(i)}) \otimes \nabla N^B(\mathbf{X}^{(i)}) \quad (18)$$

Introducing the above mentioned inner potential function

$$V^{(i),\text{int}}(\mathbf{q}^{(i)}) = \int_{\mathcal{B}^{(i)}} W(\mathbf{C}^{(i),h}) dV \quad (19)$$

using a local strain energy density function $W(\mathbf{C}^{(i),h})$ and assuming the existence of an external potential energy function

$$V^{(i),\text{ext}}(\mathbf{q}^{(i)}) = \sum_{A \in \omega^{(i)}} \mathbf{q}_A^{(i)} \cdot \left(\int_{\mathcal{B}^{(i)}} N^A \mathbf{B}^{(i)} dV + \int_{\Gamma_\sigma^{(i)}} N^A \bar{\mathbf{T}}^{(i)} d\Gamma \right) \quad (20)$$

the discrete virtual work expression can now be written as

$$G^{(i),\text{int}}(\boldsymbol{\varphi}^{(i),h}, \delta\boldsymbol{\varphi}^{(i),h}) = \sum_{A, B \in \omega^{(i)}} \delta\mathbf{q}_A^{(i)} \cdot \mathbf{q}_B^{(i)} \int_{\mathcal{B}^{(i)}} \nabla N^A(\mathbf{X}^{(i)}) \cdot \mathbf{S}(\mathbf{C}^{(i),h}) \nabla N^B(\mathbf{X}^{(i)}) dV \quad (21)$$

where $\mathbf{S}(\mathbf{C}^{(i),h}) = 2\partial W/\partial \mathbf{C}^{(i),h}$ denotes the second Piola-Kirchhoff stress tensor. The discrete virtual work expression for the external contributions reads

$$G^{(i),\text{ext}}(\boldsymbol{\varphi}^{(i),h}, \delta\boldsymbol{\varphi}^{(i),h}) = \nabla V^{(i),\text{ext}}(\mathbf{q}^{(i)}) \cdot \delta\mathbf{q}^{(i)} \quad (22)$$

Equations of motion Once again, we have to solve the non-linear system using a Newton-Raphson iteration and apply an implicit time-stepping scheme. Accordingly, the full discrete equations read

$$\begin{aligned} \mathbf{q}_{n+1} - \mathbf{q}_n &= \frac{\Delta t}{2}(\mathbf{v}_{n+1} + \mathbf{v}_n) \\ \mathbf{M}(\mathbf{v}_{n+1} - \mathbf{v}_n) &= -\Delta t[\nabla V^{(i),\text{int}}(\mathbf{q}_n, \mathbf{q}_{n+1}) - \nabla V^{(i),\text{ext}}(\mathbf{q}_n, \mathbf{q}_{n+1})] \end{aligned} \quad (23)$$

As before, each discrete body i is represented by a single object which knows its position and its contributions to the residual vector. Since we use a unified representation of the equations of motion we can simply assemble all contributions to the residual vector and add – if necessary – additional holonomic constraints to connect the bodies. Additional inequality constraints, e.g. contact constraints can be assembled similarly, for details see Hesch & Betsch [14, 13].

3 Fluid-structure interaction

As usual, we write the fluid system in terms of an Eulerian description using the inverse mapping $\mathbf{X} = \boldsymbol{\varphi}^{-1}(\mathbf{x}(t), t)$. For the time differential of a physical quantity $f(\mathbf{x}(t), t)$, it follows immediately that

$$\dot{f} = \frac{\partial f}{\partial t} + \mathbf{v} \cdot \nabla_{\mathbf{x}} f \quad (24)$$

where $\mathbf{v}(\mathbf{x}(t), t) = \partial\boldsymbol{\varphi}/\partial t$ denotes the velocity at a specific point. Without loss of generality we restrict ourself to the incompressible case and obtain for the continuity condition

$$\nabla_{\mathbf{x}} \cdot \mathbf{v} = \frac{1}{J} \dot{J} \equiv 0 \quad (25)$$

where $J = \det(\mathbf{F})$ and $\mathbf{F} : \mathcal{B} \times [0, T] \rightarrow \mathbb{R}^{d \times d}$, $\mathbf{F} = D\boldsymbol{\varphi}$ denotes the deformation gradient. For a Newtonian fluid the Cauchy stress tensor $\boldsymbol{\sigma} : \mathcal{B} \times [0, T] \rightarrow \mathbb{R}^{d \times d}$ is defined by

$$\boldsymbol{\sigma} = -p\mathbf{I} + \lambda \nabla_{\mathbf{x}} \cdot \mathbf{v} + \mu (\nabla_{\mathbf{x}} \mathbf{v} + \nabla_{\mathbf{x}}^T \mathbf{v}^T) \quad (26)$$

Here, the pressure $p : \mathcal{B} \times [0, T] \rightarrow \mathbb{R}$ is a sufficient smooth function and can be regarded as Lagrange multiplier to enforce (25). Note that for incompressible fluids the second term on the right hand side vanishes. Furthermore, μ denotes the dynamic viscosity and λ the second coefficient of viscosity. The Eulerian form of the balance of linear momentum reads

$$\rho \dot{\mathbf{v}} = \nabla_{\mathbf{x}} \cdot \boldsymbol{\sigma} + \rho \mathbf{g} \quad (27)$$

where ρ denotes the density and \mathbf{g} a prescribed body force. In weak form, the balance equation reads

$$\langle \rho(\dot{\mathbf{v}} - \mathbf{g}), \delta \mathbf{v} \rangle + \langle \boldsymbol{\sigma}, \nabla_{\mathbf{x}} (\delta \mathbf{v}) \rangle - \langle \mathbf{h}, \delta \mathbf{v} \rangle_{\Gamma^h} = 0 \quad (28)$$

supplemented by the constraints

$$\langle \nabla_{\mathbf{x}} \cdot \mathbf{v}, \delta p \rangle = 0 \quad (29)$$

As usual, we introduce suitable spaces of test functions for the velocity as well as for the pressure field

$$\begin{aligned} \mathbb{V}^v &=: \{ \delta \mathbf{v} \in \mathbb{H}^1(\mathcal{B}) \mid \delta \mathbf{v} = \mathbf{0} \text{ on } \Gamma^u \} \\ \mathbb{V}^p &=: \{ \delta p \in L_2(\mathcal{B}) \} \end{aligned} \quad (30)$$

where the Sobolev space \mathbb{H}^1 contains the set of square integrable functions and their square integrable first derivative.

Immersed solids For the calculation of fluid-structure interactions we immerse a solid system within the fluid (see Liu et al. [17]). To embed the resulting forces of the solid system, occupying the domain \mathcal{B}_t^s at time t as volumetric force $\mathcal{F} : \mathcal{B}_t^s \times [0, T] \rightarrow \mathbb{R}^d$ within the balance of linear momentum of the fluid, we reformulate (27) as follows*

$$\rho^f \dot{\mathbf{v}} = \nabla_{\mathbf{x}} \cdot \boldsymbol{\sigma}^f + \rho^f \mathbf{g} + \mathcal{F} \quad (31)$$

The force field of the immersed solid reads

$$\mathcal{F} = \begin{cases} \mathbf{0} & \text{in } \mathcal{B} \setminus \mathcal{B}^s \\ (\rho^f - \rho^s)(\dot{\mathbf{v}} - \mathbf{g}) + \nabla \cdot (\boldsymbol{\sigma}^s - \boldsymbol{\sigma}^f) & \text{in } \mathcal{B}^s \end{cases} \quad (32)$$

Next we postulate the existence of a hyperelastic constitutive law for the calculation of the solid stress field by introducing a scalar valued local strain energy function $W(\mathbf{C})$, where $\mathbf{C} = \mathbf{F}^T \mathbf{F}$ denotes the right Cauchy-Green tensor. In general, additional internal variables can be used as well for the immersed solid to include plastic or viscoelastic behavior. We obtain the actual stress field of the solid via push forward of the purely material derivative of the strain energy function

$$\boldsymbol{\sigma}^s = \frac{2}{J} \mathbf{F} \cdot \frac{\partial W(\mathbf{C})}{\partial \mathbf{C}} \mathbf{F}^T \quad (33)$$

Due to its physical properties it is convenient to use a Lagrangian mapping for the immersed solid, whereas the fluid uses an Eulerian mapping. This necessitates the definition of an Euler-Lagrange mapping $\mathcal{I}_{\mathcal{B}_t^s}$ for any given function ψ of the solid system, occupying area $\mathcal{B}_t^s \subset \mathcal{B}$ such that $\psi(\mathbf{x}, t) : \mathcal{B}_t^s \times [0, T]$ maps to $\mathcal{I}_{\mathcal{B}_t^s}(\psi(\mathbf{X}, t)) : \mathcal{B}_0^s \times [0, T]$. This motivates the mapping

$$\mathbf{v}(\mathbf{x}(t), t) = \mathcal{I}_{\mathcal{B}_t^s}(\mathbf{v}(\mathbf{X}, t)) \quad (34)$$

To complete the set of equations we define appropriate Dirichlet boundary conditions for the immersed solid

$$\mathbf{x}(\mathbf{X}, t) = \mathbf{x}_0, \quad \text{on } \partial \mathcal{B}_D^s \quad (35)$$

Since the immersed solid is surrounded by the fluid, additional Neumann boundary conditions are not treated explicitly. The corresponding weak form reads

$$\langle \rho^f (\dot{\mathbf{v}} - \mathbf{g}) - \mathcal{F}, \delta \mathbf{v} \rangle + \langle \boldsymbol{\sigma}^f, \nabla_{\mathbf{x}} (\delta \mathbf{v}) \rangle - \langle \mathbf{h}, \delta \mathbf{v} \rangle_{\Gamma^h} = 0 \quad (36)$$

and for the constraints

$$\langle \nabla_{\mathbf{x}} \cdot \mathbf{v}, \delta p \rangle = 0 \quad (37)$$

It is convenient to rewrite the solid system within the material domain. Using $J^s = \det(\mathbf{F}^s)$ and the notation

$$\int_{\mathcal{B}_0^s} (\bullet) \cdot (\bullet) dV =: \langle \bullet, \bullet \rangle_0^s \quad (38)$$

*Contributions to the solid system are marked with $(\bullet)^s$, whereas contributions to the fluid are marked with $(\bullet)^f$.

in addition to the Euler-Lagrange mapping, we obtain for the balance equations

$$\begin{aligned}
& \langle \rho^f (\dot{\mathbf{v}} - \mathbf{g}), \delta \mathbf{v} \rangle + \langle \boldsymbol{\sigma}^f, \nabla_{\mathbf{x}} (\delta \mathbf{v}) \rangle - \langle \mathbf{h}, \delta \mathbf{v} \rangle_{\Gamma^h} \\
& - \langle (\rho^f - \rho^s) \left(\frac{\partial}{\partial t} \mathcal{I}_{\mathcal{B}_i^s}(\mathbf{v}(\mathbf{X}, t)) - \mathbf{g} \right), \mathcal{I}_{\mathcal{B}_i^s}(\delta \mathbf{v}) J^s \rangle_0^s \\
& - \langle \boldsymbol{\sigma}^s - \boldsymbol{\sigma}^f, \nabla_{\mathbf{x}} \mathcal{I}_{\mathcal{B}_i^s}(\delta \mathbf{v}) J^s \rangle_0^s = 0
\end{aligned} \tag{39}$$

As before we subdivide the area into finite elements and apply appropriate shape functions and obtain

$$\begin{aligned}
\mathbf{v}^h &= \sum_{A \in \omega} N^A \mathbf{v}_A; & \delta \mathbf{v}^h &= \sum_{A \in \omega} N^A \delta \mathbf{v}_A \\
p^h &= \sum_{B \in \bar{\omega}} M^B p_B; & \delta p^h &= \sum_{B \in \bar{\omega}} M^B \delta p_B
\end{aligned} \tag{40}$$

where $N^A(\mathbf{x}) : \mathcal{B}^h \rightarrow \mathbb{R}$ are quadratic shape functions associated with nodes $A \in \omega = \{1, \dots, n\}$ and $M^B(\mathbf{x}) : \mathcal{B}^h \rightarrow \mathbb{R}$ are linear shape functions associated with nodes $B \in \bar{\omega} = \{1, \dots, m\}$. This element satisfies the LBB condition and provides optimal quadratic convergence of the velocity field (see Donea & Huerta [8]). The semi-discrete balance of momentum reads

$$\langle \rho^f (\dot{\mathbf{v}}^h - \mathbf{g}^h), \delta \mathbf{v}^h \rangle + \langle \boldsymbol{\sigma}^f(\mathbf{v}^h, p^h), \nabla_{\mathbf{x}} (\delta \mathbf{v}^h) \rangle - \langle \mathbf{h}^h, \delta \mathbf{v}^h \rangle_{\Gamma^h} = 0 \tag{41}$$

whereas the constraints reads

$$\langle \nabla_{\mathbf{x}} \cdot \mathbf{v}^h, \delta p^h \rangle = 0 \tag{42}$$

Equations of motion At last, the full discrete equations of motions for the fluid reads

$$\begin{aligned}
\langle \rho \left(\frac{\mathbf{v}_{n+1}^h - \mathbf{v}_n^h}{\Delta t} - (\mathbf{v}_{n+1/2}^h \cdot \nabla_{\mathbf{x}}) \mathbf{v}_{n+1/2}^h - \mathbf{g}_{n+1/2}^h \right), \delta \mathbf{v}^h \rangle + \\
\langle \boldsymbol{\sigma}(\mathbf{v}_{n+1/2}^h, p_{n+1}^h), \nabla_{\mathbf{x}} (\delta \mathbf{v}^h) \rangle - \langle \mathbf{h}_{n+1/2}^h, \delta \mathbf{v}^h \rangle_{\Gamma^h} = 0 \\
\langle \nabla_{\mathbf{x}} \cdot \mathbf{v}_{n+1}^h, \delta p^h \rangle = 0
\end{aligned} \tag{43}$$

The additional contributions for the immersed contributions have to be discretized in time as well and we obtain for the contributions of the balance equation

$$\begin{aligned}
\mathcal{F}^h(\mathbf{v}_n, \mathbf{v}_{n+1}, p_{n+1}) = \\
- \langle (\rho_0^f - \rho_0^s) \left(\frac{\mathcal{I}_{\Omega^s}(\mathbf{v}_{n+1}^h) - \mathcal{I}_{\Omega^s}(\mathbf{v}_n^h)}{\Delta t} - \mathbf{g}_{n+1/2}^h \right), \mathcal{I}_{\Omega^s}(\delta \tilde{\mathbf{v}}^h) \rangle_0^s \\
- \langle \mathbf{S}^s, (\mathbf{F}^s(\mathcal{I}_{\Omega^s}(\mathbf{v}_{n+1/2}^h)))^T \nabla_{\mathbf{X}} \mathcal{I}_{\Omega^s}(\delta \tilde{\mathbf{v}}^h) \rangle_0^s \\
+ \langle \boldsymbol{\sigma}^f(\mathcal{I}_{\Omega^s}(\mathbf{v}_{n+1/2}^h), \mathcal{I}_{\Omega^s}(p_{n+1}^h)), \nabla_{\mathbf{x}} \mathcal{I}_{\Omega^s}(\delta \tilde{\mathbf{v}}^h) J^s(\mathcal{I}_{\Omega^s}(\mathbf{v}_{n+1/2}^h)) \rangle_0^s
\end{aligned} \tag{44}$$

For further details on immersed techniques see Hesch et al. [15]. As before, the fluid as well as the immersed solid are treated as separate objects. Note that the contributions for the residual vector of the immersed object are distributed to the corresponding contributions of the fluid nodes.

4 Examples

4.1 Rigid bodies

The first example deals with a three dimensional rotary crane (Fig. 1). The crane has five degrees of freedom and has been originally formulated in terms of generalized coordinates. It is comprised of three rigid bodies. In particular, the girder bridge (body 1) is connected to the trolley (body 2) via a prismatic joint. A revolute joint couples the trolley with the winch (body 3). A mass point (body 4) is applied as load.

Accordingly, the present approach yields $n = 42$ coordinates subject to $m = 37$ holonomic constraints. The inertia properties of the multibody system at hand are summarized in Table 1. Additionally, the initial

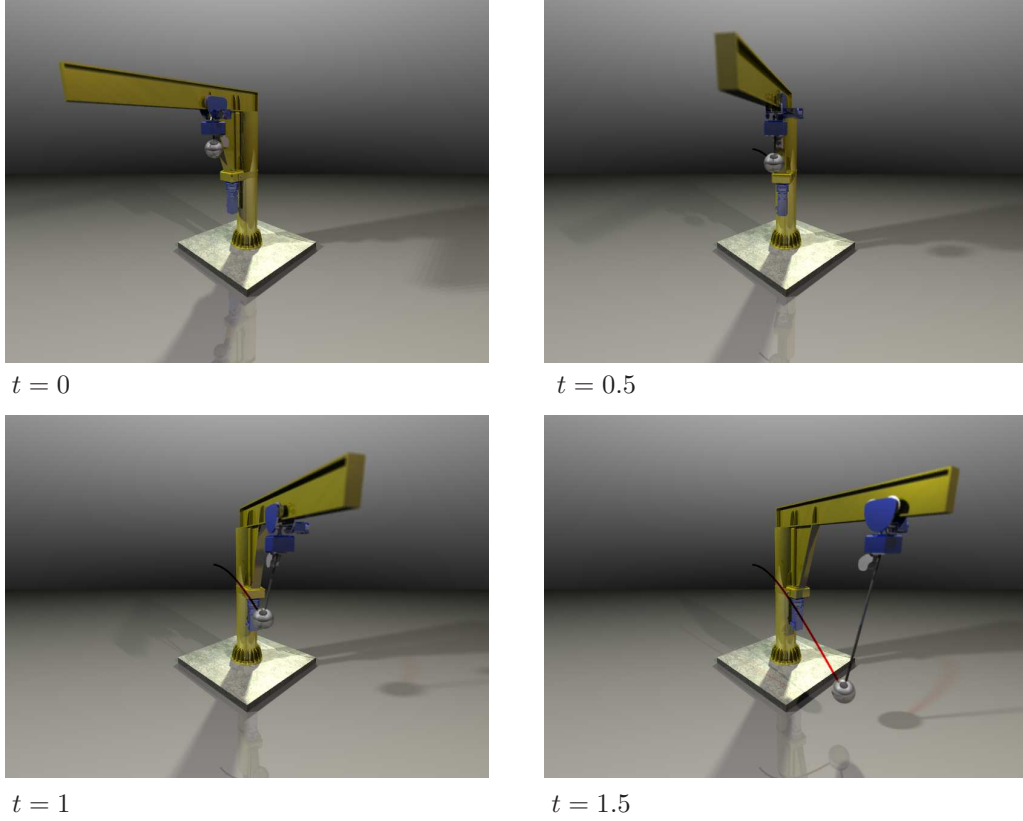


Figure 1. Rotary crane: Snapshots of the motion.

length of the rope, connecting the winch to the load mass, is $L_0 = 1.2$, and the winch radius is $r_w = 0.1$. Gravity is acting on the system with $g = 9.81$. In the initial configuration the distance between the trolley and the crane axis of rotation is $u_0 = 1.5$, and the rope is parallel to the crane axis of rotation. The initial velocity of the system is characterized by an angular velocity of $\omega_0 = 1.32$ about the crane axis of rotation.

Table 1. Inertia data for the rotary crane.

body	mass	\mathcal{E}_1	\mathcal{E}_2	\mathcal{E}_3
1	100	8.3	208.3	8.3
2	50	1.0417	1.0417	1.0417
3	3	0.01	0.01	0.25
4	10	–	–	–

The multibody system under consideration is conservative and has a rotational symmetry about the crane axis of rotation. Accordingly, the total energy as well as the 3-component of the total angular momentum are conserved quantities (see Betsch et al. [3]).

4.2 Deformable bodies

The next example deals with an impact simulation of two tori. The configurations after certain time-steps are shown in Fig. 2 Both tori are discretized using 8024 eight-node brick elements with overall 72216 degrees of freedom. The inner and outer radii are 52 and 100 respectively, the wall thickness of each hollow torus is 4.5. A standard Neo-Hookean hyperelastic material with $\mathcal{E} = 2250$ and $\nu = 0.3$ is used. The initial density $\rho = 0.1$ and the homogeneous, initial velocity of the left torus is given by $v = [30, 0, 23]$. A time-step size of $\Delta t = 0.01$ has been used for this approach, using a mortar based segmentation procedure to interpolate the stress field within the actual contact area.

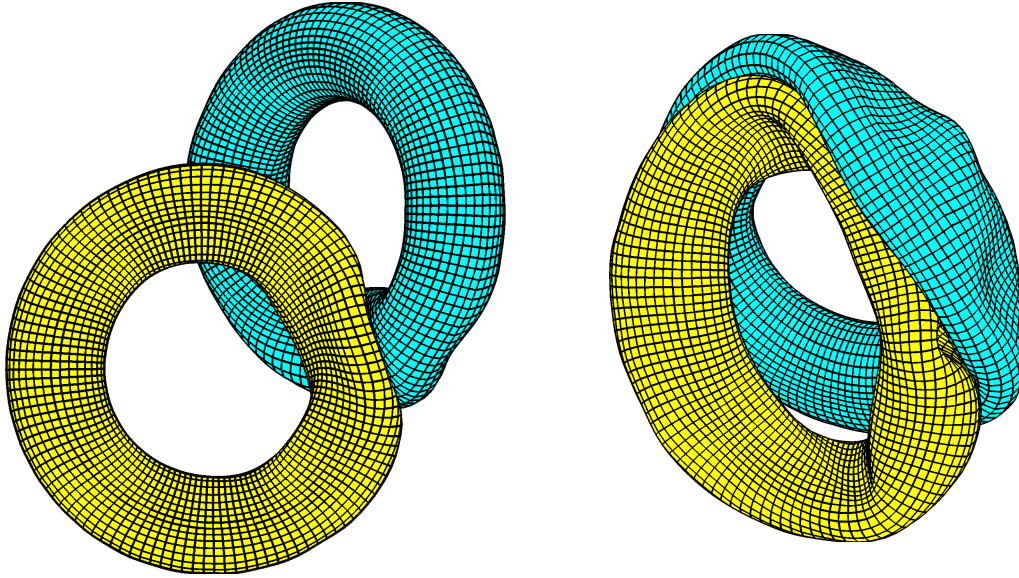


Figure 2. Configurations at time $t = 2$ and $t = 5$.

4.3 Fluid-structure interaction

The last example deals with the application of immersed techniques to cardiovascular problems. Therefore, we consider blood as incompressible Newtonian viscous fluid with viscosity $\mu = 1$ and density $\rho = 1 \cdot 10^5$. Two flaps are inserted into the channel, see Fig. 3, the top and the bottom sides are fixed and a Poiseuille inflow is applied to the left using the amplitude function $A(t) = 5 \cdot (\sin(2\pi t) + 1.1)$ and no boundary conditions are imposed to the right hand side. The flaps are modeled as Neo-Hookian solids using the Lamé parameters $\lambda^s = 8 \cdot 10^6$ and $\mu^s = 2 \cdot 10^6$ corresponding to a Young's modulus of $E = 5.6 \cdot 10^6$ and a Poisson ratio of $\nu = 0.4$. They can be regarded as idealization of a human heart valve exposed to insufficiency modeled by the gap between both flaps, cf. Gil et al. [9]. The series of figures in Fig. 4 shows

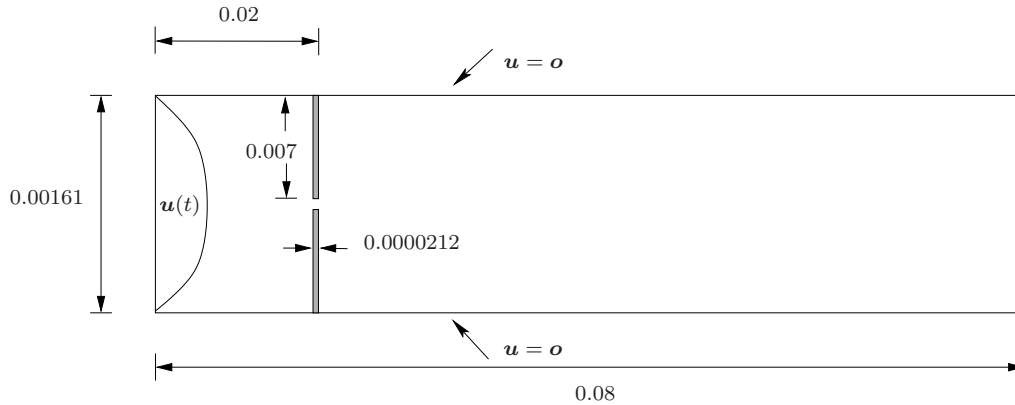


Figure 3. Geometry and boundary conditions for two flapping membranes.

the time evolution for the pulsatile flow using 256x64 Q1Q1 fluid and 40x4 linear solid elements.

5 CONCLUSIONS

We have shown how to incorporate different mechanical systems within a single theoretical as well as implementation framework. Based on rotationless formulations for rigid bodies and finite element based discretizations of deformable bodies and fluid systems we receive a common structure of differential algebraic equations. Although not shown, the same theoretical framework can be extended to geometrically exact

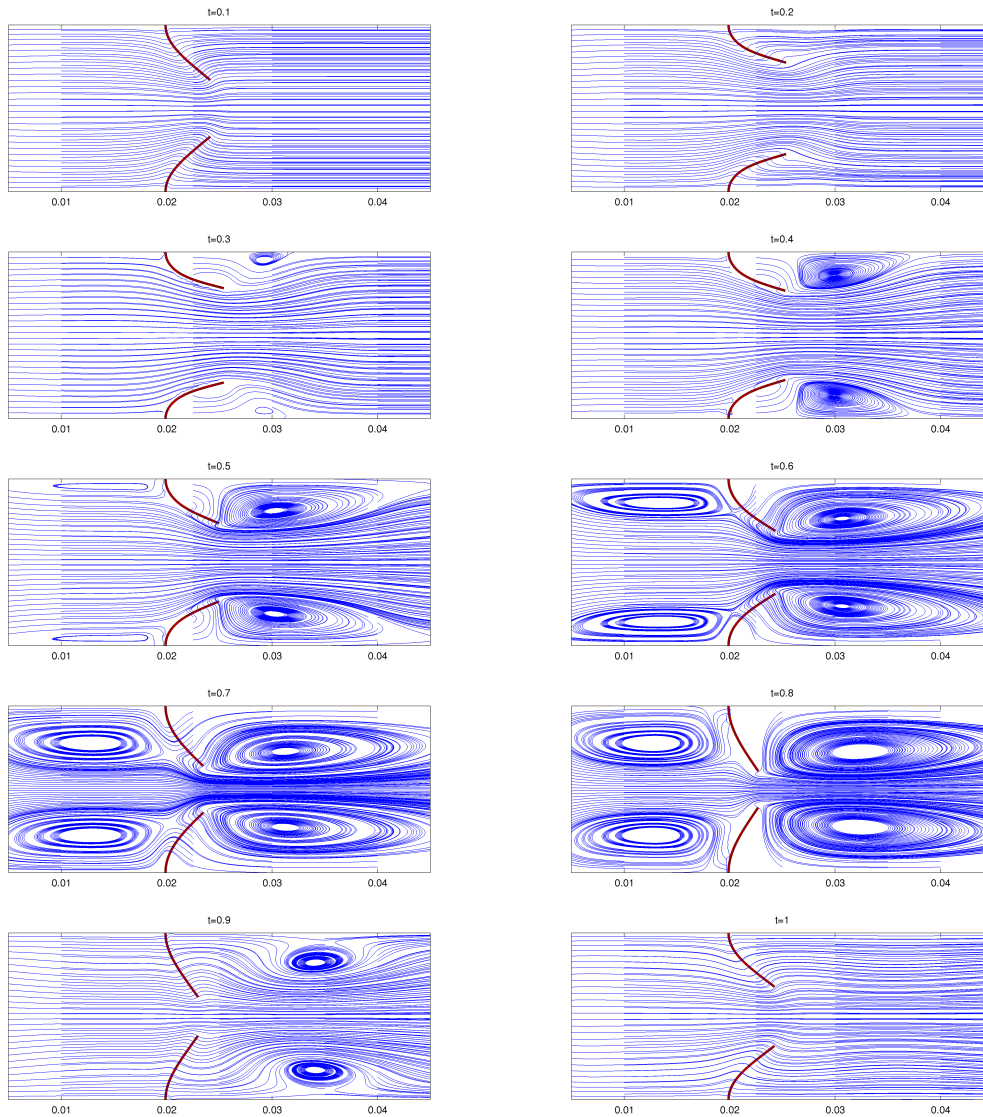


Figure 4. Time evolution of the membranes and streamlines of the fluid.

beams and shells. This common structure can be easily implemented in a single object oriented framework and allows us an efficient usage of the different objects.

REFERENCES

- [1] D. Anders, C. Hesch, and K. Weinberg. Computational modeling of phase separation and coarsening in solder alloys. *Int. J. Solids Structures*, 2012. accepted for publication.
- [2] P. Betsch. The discrete null space method for the energy consistent integration of constrained mechanical systems Part I: Holonomic constraints. *Comput. Methods Appl. Mech. Engrg.*, 194:5159–5190, 2005.
- [3] P. Betsch, C. Hesch, N. Sanger, and S. Uhlar. Variational integrators and energy-momentum schemes for flexible multibody dynamics. *Journal of Computational and Nonlinear Dynamics*, 5(3), March 2010.
- [4] P. Betsch and N. Sanger. On the use of geometrically exact shells in a conserving framework for flexible multibody dynamics. *Comput. Methods Appl. Mech. Engrg.*, 198:1609–1630, 2009.

- [5] P. Betsch and P. Steinmann. Frame-indifferent beam finite elements based upon the geometrically exact beam theory. *Int. J. Numer. Methods Eng.*, 54:1775–1788, 2002.
- [6] P. Betsch and S. Uhlar. Energy-momentum conserving integration of multibody dynamics. *Multibody System Dynamics*, 17(4):243–289, 2007.
- [7] P. Betsch and S. Uhlar. A rotationless formulation of multibody dynamics: Modeling of screw joints and incorporation of control constraints. *Multibody System Dynamics*, 22:69–95, 2009.
- [8] J. Donea and A. Huerta. *Finite element methods for flow problems*. John Wiley & Sons, 2003.
- [9] A.J. Gil, A. Arranz Carreño, J. Bonet, and O. Hassan. The immersed structural potential method for haemodynamic applications. *Journal of Computational Physics*, 229:8613–8641, 2010.
- [10] C. Hesch and P. Betsch. A mortar method for energy-momentum conserving schemes in frictionless dynamic contact problems. *Int. J. Numer. Methods Eng.*, 77:1468–1500, 2009.
- [11] C. Hesch and P. Betsch. Transient 3D Domain Decomposition Problems: Frame-indifferent mortar constraints and conserving integration. *Int. J. Numer. Methods Eng.*, 82:329–358, 2010.
- [12] C. Hesch and P. Betsch. Energy-momentum consistent algorithms for dynamic thermomechanical problems - application to mortar domain decomposition problems. *Int. J. Numer. Methods Eng.*, 86:1277–1302, 2011.
- [13] C. Hesch and P. Betsch. Transient 3d contact problems – Mortar method: Mixed methods and conserving integration. *Computational Mechanics*, 48:461–475, 2011.
- [14] C. Hesch and P. Betsch. Transient 3d contact problems – NTS method: Mixed methods and conserving integration. *Computational Mechanics*, 48:437–449, 2011.
- [15] C. Hesch, A.J. Gil, A. Arranz Carreño, and J. Bonet. On immersed techniques for fluid-structure interaction. *Comput. Methods Appl. Mech. Engrg.*, 2012. submitted.
- [16] M. Krüger, M. Groß, and P. Betsch. A comparison of structure-preserving integrators for discrete thermoelastic systems. *Computational Mechanics*, 47(6):701–722, 2011.
- [17] L. Zhang, A. Gerstenberger, X. Wang, and W.K. Liu. Immersed finite element method. *Comput. Methods Appl. Mech. Engrg.*, 193:2051–2067, 2004.